A VERSATILE PLATFORM FOR MULTIMODALITY IMAGING OF PANCREATIC TUMOR BY TARGETING P-SELECTIN

by

Jiaqi Lu

A thesis submitted to Johns Hopkins University in conformity with the requirements for the degree of Master of Science and Engineering

Baltimore, Maryland
May, 2019

Abstract

Background

Pancreatic ductal adenocarcinoma (PDAC) is one of the most lethal human malignancies. Due to the lack of early disease-specific signs and symptoms, early detection of pancreatic cancer is really difficult. Detection of preinvasive pancreatic cancer are paramount to improving the survival of patients.

Methods

In our study, we developed a versatile platform for multimodality imaging of PDAC. The system consists of dibenzocyclooctyne (DBCO)-functionalized fucoidan particles (fucoidan-DBCO), which target a tumor microenvironment biomarker, P-selectin, allows in vivo click reaction with azide-functionalized fluorescence dye, gadolinium chelates, iron oxide particles, and dextran particles, for fluorescence imaging, T1-weigthed, T2*-weighted MRI and chemical exchange saturation transfer (CEST) MRI respectively. The system was applied in a two-step manner, where fucoidan-DBCO particles were firstly injected, followed by injection of azide-functionalized imaging probes.

We first confirmed the overexpression of P-selectin in a murine PDAC model, derived from $Kras^{LSL.G12D/+}$; $P53^{R172H/+}$; $Pdx^{Cretg/+}$ (KPC) mice, using immunofluorescence staining. We next synthesized fucoidan-DBCO, which is reactive to azide-functionalized Cy5.5 fluorescent dye, Gd(DOTA), superparamagnetic iron oxide particles (SPIO), and dextran particles through in vivo click reaction. We also evaluated the R1, R2 relaxivity of azide-Gd(DOTA) and azide-

SPIO, and the CEST signal of fucoidan-DBCO and dextran-azide in vitro. Reaction between fucoidan-DBCO and azide-Gd(DOTA) was validated by the increase in relaxivity. KPC mice were intravenously injected with fucoidan-DBO, followed by injection of azide-Cy5.5 after 1 hour to test the enhancement of tumor targeting in ex vivo fluorescence imaging. T1-weigthed MRI and T1-mapping was also performed in mice with serial injection of fucoidan-DBCO and azide-Gd(DOTA). KPC mice without fucoidan-DBCO injection was used as controls.

Results

Higher P-selectin expression was observed in KPC tumors than muscles (P=0.001). Mice with fucoidan-DBCO injection demonstrated ~50% higher tumor enhancement after injection of azide-Cy5.5 in ex vivo fluorescence imaging, compared with control mice (P=0.048, n=3). After adding fucoidan-DBCO, the R1 relaxivity of azide-Gd(DOTA) increased from 2.12 $mM^{-1}s^{-1}$ to 3.68 $mM^{-1}s^{-1}$. In MRI, higher tumor enhancement was also observed in mice with serial fucoidan-DBCO injection and azide-Gd(DOTA) injection than those with only azide-Gd(DOTA) injection.

Conclusions

We provided a versatile platform for multimodality imaging of PDAC.

Advisor: Dr. Guanshu Liu (co-advisor: Dr. Joelle Frechette)

Acknowledgments

I entered in Johns Hopkins University in 2017, driven by strong interest in improving human health, I participated in Dr. Guanshu Liu's research group soon after I started my master program. From the courses and research in the two short years, I gained a lot of research experience and skills. Besides, I had tremendous opportunity to meet and interact with wonderful faculty members and students from Chemical and Biomolecular Engineering department and Radiology Department. I was really honored to get to know and work with every one of you.

First, this work would not be possibly achieved without my advisor, Dr. Guanshu Liu. I have learnt not only how to actively solve a problem in science, but also how to make simple presentations to demonstrate my results. Moreover, Dr. Liu offered me many opportunities to attend academic conferences and meetings, such as Radiology Retreat and ISMRM Annual Meeting.

Next, I would like to thank my fellow lab members and post-docs, Dr. Zheng Han, Dr. Jia Zhang, Dr. Yuguo Li, Dr. Shaowei Bo, Chuheng Chen and Zelong Chen. They are great sources of direction, collaborations and friendship. Especially, Zheng gave very thoughtful and thorough guidance to my experiments, and I learnt tremendous experiment skills, for example, animal vein injection, cell culture, slices staining, which are brand new for me. A very large part of my experiments mentioned in this thesis were achieved successfully because of their collaborations and superior teaching skills, and I was gracious enough to follow their footsteps.

Besides, I would like to thank my parents and my other families. They always support and encourage me when I decided to pursue a higher education to achieve my career goal.

Finally, I would like to thank all my friends and professors I had a chance to interact with both academically and personally, so that I can become a better academic and a better person.

Content

1. Introduction 1

1.1 Molecular Imaging of PDAC 1

1.2 P-selectin as a cancer biomarker 2

1.3 CEST MRI for cancer detection 3

1.4 Dextran as a CEST MRI probe for cancer detection 5

1.5 T_1 and T_2 MRI agents 6

1.6 Relaxivity and safety of Gd (III)-DOTA 8

1.7 Fucoidan 9

1.8 Summary 11

2. Experimental Methods 12

2.1 Synthesis 12

2.1.1 Materials 12

2.1.2 Synthesis Method of Dextran-N_3 12

2.1.3 Synthesis Method of Fucoidan-DBCO 12

2.2 In Vitro CEST of Dex10, Dex10-N_3, Fucoidan and Fucoidan-DBCO 14

2.2.1 Preparation of Samples for MR Imaging 14

2.2.2 MRI Measurement and Analysis 14

2.3 Histological Analysis of P-selectin Expression in tumor and muscle 16

2.3.1. Immunohistochemistry (IHC) Staining Protocol 16

2.4 Ex Vivo Fluorescence Imaging 17

2.4.1 Cell Culture 17

2.4.2 The KPC Model of Pancreatic Ductal Adenocarcinoma 18

2.4.3 Animal Model 18

2.4.4 Fluorescence Imaging Analysis 19

2.5 Relaxivity of Gd(DOTA)-N_3 20

2.5.1 Chelation Reaction of T_1 Agent Gd(DOTA)-N_3 20

2.5.2 Chelation of T_2 Agent SPIO-N_3 21

2.5.3 T_1 and T_2 of Gd(DOTA)-N_3 21

2.6 In Vivo MRI with Azide-Gd(DOTA) 22

3. Results 24

3.1 Synthesis of Dextran-N_3 and Fucoidan-DBCO 24

3.2 In Vitro CEST Results 24

3.3 Histological Analysis of P-selectin Expression in tumor and muscle 25

3.4 Ex Vivo Fluorescence Imaging 27

3.5 Relaxivities of Gd(DOTA)-N_3 30

3.5.1 The productivity of Gd (DOTA)-N_3 Chelation Reaction 30

3.5.3 In vivo MRI of PDAC using Gd(DOTA)-N_3 31

4. Discussion 33

5. References 35

List of figures

Figure 1.1 Mechanism of CEST from RF Irradiation to Measurement and Analysis. Solute proton exchanges RF irradiation with bulk water. ^{1}H spectra are taken before and after saturation equilibrium. Then, the spectra are normalized and its frequency difference is used to generate MTR_{asym}.[12] 4

Figure 1.2 (a) Chemical structure of dextran and (b) ball-and-stick model of dextran molecule [13]. 5

Figure 1.3 Structures of the Gd(III) based MRI contrast agents currently used in the clinical practice.[29] 8

Figure 1.4 Typical structure of fucoidan (FCSPs) obtained from some brown seaweed species in the order of Fucales [43]. 10

Figure 2.1 Scheme of Synthesis Route of (a) Dextran-N_3 and (b) Fucoidan-DBCO 13

Figure 2.2 Scheme of Ex vivo Fluorescence Imaging. 19

Figure 2.3 Scheme of In Vivo T1 & T2 Scan 23

Figure 3.1 In vitro CEST of fucoidan and dextran. 25

Figure 3.2 Immunohistochemistry (IHC) Analysis of P-selectin Expression in (a) Tumors and (b) Muscles. 25

Figure 3.3 Quantification of P-selectin Expression in Tumors and Muscles (N=3, two-tailed unpaired Student's test, based on whole-tumor ROI) 26

Figure 3.4 Chemical Structure of Sulfo-Cy5.5-N_3 27

Figure 3.5 Schematic of the tumor position 28

Figure 3.6 Localization of cy5.5-azide localization to mice by ex-vivo fluorescence imaging. .. 29

Figure 3.7 Fluorescence Intensity in all organs and muscle and KPC tumor of mice. (N=3, two-tailed unpaired Student's test, based on whole-tumor ROI) 29

Figure 3.8 (a) Chemical Structure of Azide-mono-amide-DOTA. The chemical name of it is 1,4,7,10-Tetraazacyclododecane-1,4,7-tris (acetic acid)-10-(Azidepropyl ethylacetamide). (b) Chemical structure of Gadolinium (III) acetate hydrate. (c) The chemical structure of Gd (DOTA)-N_3. 30

Figure 3.9 R1 relaxation rates of Gd(DOTA)-N_3 with or without adding fucoidan-DBCO. 30

Figure 3.10 (a) T_1-weighted MRI of PDAC using Gd(DOTA)-N_3. (b) Plots of in vivo MRI of tumor and muscle 31

1. Introduction

This section introduces the aim of our study: developing a molecular imaging platform of PDAC, and the different components of our multimodality imaging platform, which consists of fucoidan as the targeting ligand for PDAC, gadolinium-chelates, superparamagnetic iron oxide particles and dextran particles, as the imaging moieties. Mechanisms of chemical exchange saturation MRI, and T_1, T_2 agents are introduced.

1.1 Molecular Imaging of PDAC

PDAC is one of the most lethal human malignancies, and accounts for 7% of all cancer-related deaths in the United States.[1] Due to the lack of early disease-specific signs and symptoms, early detection of pancreatic intraepithelial neoplasia (PanIN) lesions and PDAC is difficult and only 10-20% of patients with pancreatic cancer are candidates for curative resection.[2] Detection of preinvasive pancreatic neoplasms are paramount to improving the survival of patients. Compared to biopsy, the current gold standard for PDAC diagnosis, imaging diagnosis of PDAC is non-invasive and not prone to errors from limited tissue sampling. However, the most commonly used imaging modalities in PDAC, computed tomography (CT) and ultrasound, only provide morphological information of the pancreas, which in some cases has limited diagnostic value. MRI has a superb soft tissue resolution and is free of ionizing radiation. However, current MRI procedures provide no information beyond morphological and semi-physiological parameters, such as perfusion, of pancreas, and MRI is only considered as secondary “problem-solving” imaging modality in addition to CT and ultrasound.[3, 4]

Molecular imaging provides an opportunity to delineate molecular changes correlated to early PDAC tumorigenesis. Tumor vasculature, which is composed of smooth muscle cells, pericytes, extracellular matrix, and endothelial cells (ECs), is necessary for the growth and support of tumors.[5] Here we aim to develop an MR molecular imaging approach for detecting PDAC by the tumor microenvironment (TME). PDAC is a micrometastatic disease and TME plays an important role in driving cancer progression.

1.2 P-selectin as a cancer biomarker

Selectins are cellular adhesion molecules expressed on the cell surface and assist in cell-cell interaction and adhesion. Selectins (E-, P-, L-selectins) were originally named due to the three membrane-anchored Ca^{2+}-dependent (C-type) lectins that bind to cell-surface carbohydrate ligands and function as adhesion molecules. Their site of expression best classifies the selectins: for example, activated endothelium (E-selectin), lymphocytes (L-selectin) and platelets (P-selectin) [6]. P-selectin is a protein that in humans is encoded by the SELP gene. P-selectin functions as a cell adhesion molecule (CAM) on the surfaces of activated endothelial cells, which line the inner surface of blood vessels, and activated platelets [7]. P-selectin facilitates metastasis by arresting tumor cells at the endothelium. P-selectin is overexpressed on cancer cells in many mice and human tumors [5]. Therefore, in this work, P-selectin was chosen as the molecular target. It has been previously demonstrated that fucoidan-functionalized nanoparticles or microparticles targeted to P-selectin can facilitate the diagnosis of endothelial activation and intraluminal thrombosis, and for tumor-targeted drug delivery.[8] The nanoparticles targeted the tumor microenvironment to localize chemotherapeutics at tumor

sites to achieve targeted specific detection of PDAC tumor.

1.3 CEST MRI for cancer detection

Chemical exchange saturation transfer (CEST) is a new and versatile MRI contrast-generating mechanism [9], proven to be sensitive to metabolites, extracellular pH, enzymatic activity, and gene expression, etc. It has demonstrated in many studies for specifically detecting a wide array of labile protons of exchange rate (k_{ex}) in the slow to intermediate range (i.e., $k_{ex} < \Delta\omega$, where $\Delta\omega$ is the chemical shift difference between the proton and water in the unit of radian). In brief, as illustrated in **Figure 1.1**, CEST is able to detect the exchangeable protons of the targeted agent (solute) through the changes in the NMR signal in water molecule. Without the saturation of the targeted proton (such as amide, hydroxide, or bound water group), the NMR proton (^1H) spectrum shows two peaks for both the solute proton and bulk water proton at different resonance frequencies (e.g., 8.25 ppm for amide and 4.75 ppm for bulk water respectively). Upon the application of Radiofrequency (RF)[10] saturation pulse irradiating at the offset of the exchangeable protons, the NMR signal of those protons will disappear. Over time, as the saturated solute protons exchange with bulk water protons to reach equilibrium, not only the signal of the solute protons remains saturated, but also a great reduction can be observed on the water signal. Plotting the normalized water signal (by its signal in the absence of RF saturation pulses) with respect to the offsets of the applied RF saturation pulses gives a so-called Z-spectrum or CEST spectrum, in which CEST signal can be directly visualized at a particular frequency offset $\Delta\omega$ defined by the distance between the chemical shift of the solute proton and that of bulk water (in ppm). It should be noted that, by MRI convention, the

frequency offset is defined as the frequency difference (Δω) between a proton and water, whereas the chemical shift of water is set to 0 whereas it is 4.7 ppm by NMR convention [11]. The CEST effect can be analyzed and quantified using magnetization transfer ratio asymmetry (MTR_{asym}), which will be elaborated in later sections.

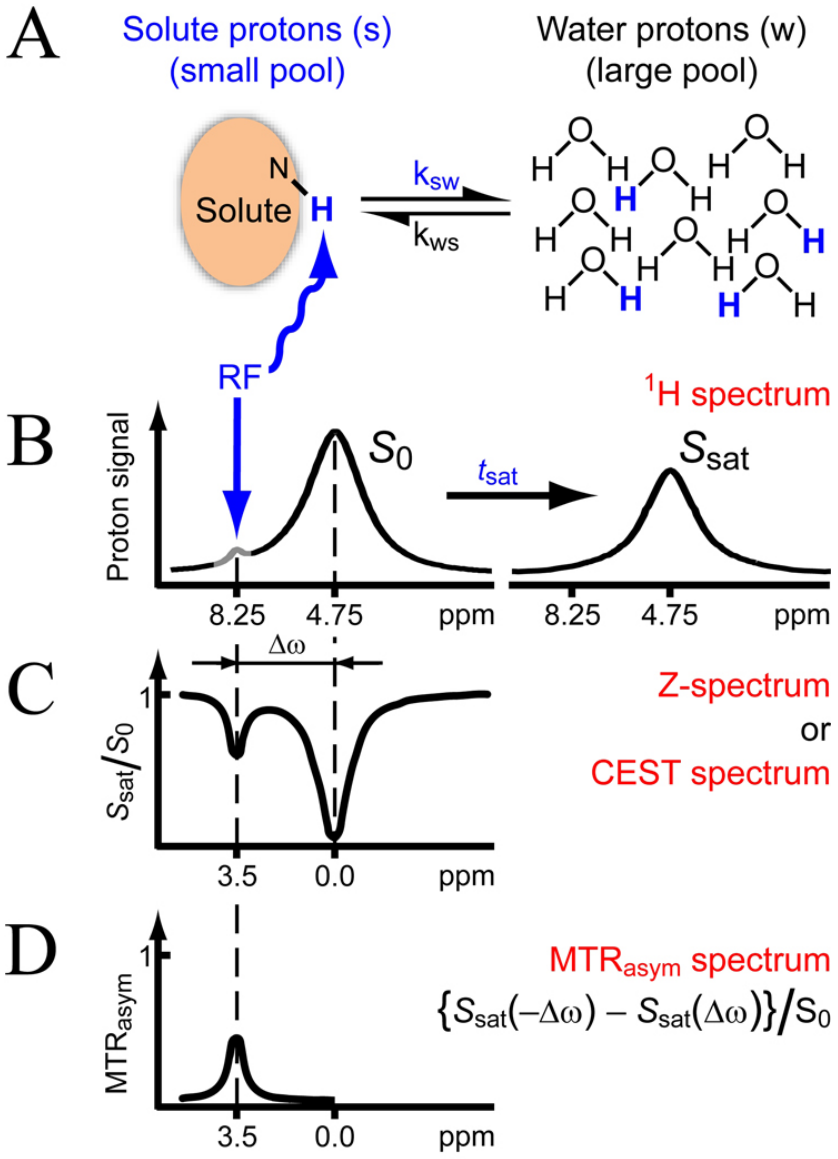

Figure 1.1 Mechanism of CEST from RF Irradiation to Measurement and Analysis. Solute proton exchanges RF irradiation with bulk water. ^{1}H spectra are taken before and after saturation equilibrium. Then, the spectra are normalized and its frequency difference is used to generate MTR_{asym}.[12]

1.4 Dextran as a CEST MRI probe for cancer detection

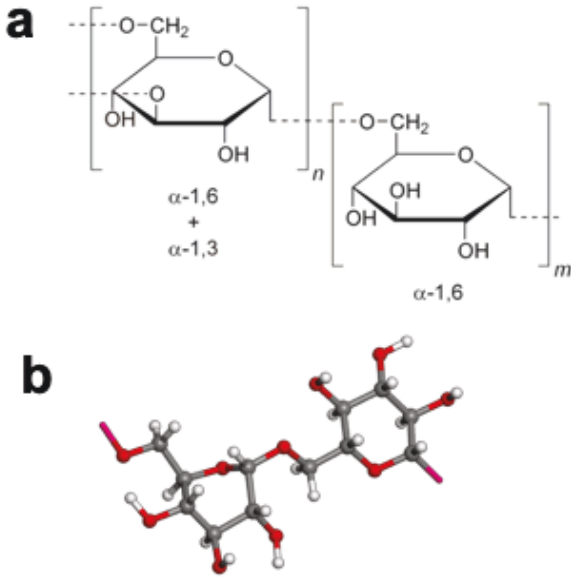

Figure 1.2 (a) Chemical structure of dextran and (b) ball-and-stick model of dextran molecule [13].

CEST agents [14, 15], which are molecules with exchangeable protons, can be divided into two classes: (i) paramagnetic CEST agents (PARACEST) and (ii) diamagnetic CEST agents. Molecules with exchangeable protons capable of providing CEST contrast combined with a paramagnetic metal ion (typically one of the lanthanides) are known as PARACEST agents. On the other hand, diamagnetic CEST agents are simply molecules with exchangeable protons, which allow for more selective irradiation and imaging of faster exchanging species.

CEST MRI portends a pathway for quick translation of new molecular imaging probes by the use of those highly biocompatible and clinically ready-to-be used compounds such as glycogen [16], glucose [17, 18], anticancer drugs,[19-21] clinical x-ray contrast agents,[22, 23] etc. Our previous studies showed that dextran, a branched polysaccharide rich in OH protons, can be detected by CEST MRI [24, 25]. Dextran of higher molecular weight has higher CEST

sensitivity on a per-dextran-unit basis, but detectability on a per-glucose-unit basis is similar to those of low-molecular-weight dextrans and glucose. Dextran efficiently facilitates tumor receptor detection and assessment of vasculature permeability in CEST MRI. In our study, we choose dextran [24], a highly biocompatible diamagnetic CEST agent, as MR molecular imaging agent for early detection of PDAC [26].

1.5 T_1 and T_2 MRI agents

Current commercially available MRI contrast agents are biocompatible magnetic materials that alter the longitudinal (T_1) and transverse (T_2) relaxation rates of the surrounding water protons, therefore enhancing image contrast in tissues of interest.[27] MRI contrast agents are generally classified as T_1 and T_2 contrast agents based on their magnetic properties and relaxation mechanisms. Gadolinium Gd (III) chelates [28, 29] effectively increase the T_1 relaxation rate ($1/T_1$) and is often used as T_1 contrast agents to produce a positive image contrast. Superparamagnetic iron oxide nanoparticles （SPIO）[30] are more effective at increasing T_2 relaxation rate ($1/T_2$) and are commonly used as T_2 contrast agents to produce negative image contrast. To date, the majority of MRI contrast agents used in clinical practice are Gd (III) chelates, with more than 10 million contrast enhanced MRI scans per year, because of their high paramagnetic properties, and favorable properties in term of enhancing relaxation enhancement, high stability and inert body.

Clinical MRI contrast agents are mostly small molecular Gd (III) chelates, and they usually have high stability. The first MRI contrast agent Gd-DTPA has been permitted to be used in clinic in 1988.[31] It was firstly used in detecting the breakage of the blood brain barrier (BBB)

in brain tumors. Afterwards, plenty of Gd (III) chetales have been developed to be used in clinic, as **Figure 1.3** shows. Macromolecular MRI contrast agents are mainly prepared by conjugated Gd-DOTA to biocompatible macromolecules. Various bifunctional chelates of DOTA have been developed with functional goups such as anhydride, N-hydroxysuccinimide activated carboxylic acis, malemide, alkynyl and azide for conjugation. Bifunctional ligands and small molecular Gd chelates can be readily attached to many biocompatible macromolecules such as proteins, polymers and dendrimers to produce macromolecular contrast agents. Although there has been superparamagnetic iron oxide nanoparticles (SPIO) which is approved by FDA for human uses, these agents are not positively accepted in the area of radiology, possibly because of negative contrast enhancement and their prolonged in vivo contrast enhancement, up to several months. Clinical Gd (III) based MRI contrast agents can offer strong positive contrast enhanement and metabolite quickly from human body after the MRI examinations.

Nowadays, Gd (III) based MRI contrast agents have been widely used in clinical practice. Targeted delivery of contrast agents into tumor tissues is crucial in cancer diagnostic MRI. Tumor is physiologically different from normal tissue and has leaky blood vasculature. Thus, nanosized contrast agents can passively accumulate in the tumor via tumor vascular permeability to macromolecules [32]. Tumor tissues also express numerous cancer-related biomarkers, such as P-selectin, on tumor cell surface, extracellular matrix or angiogenic microvessels, which can be targeted for molecular imaging. Abundantly expressed cancer biomarkers and ligands with high-binding affinity are essential for designing targeted contrast agents in order to generate sufficient contrast enhancement for visualizing these biomarkers with contrast enhanced MRI.

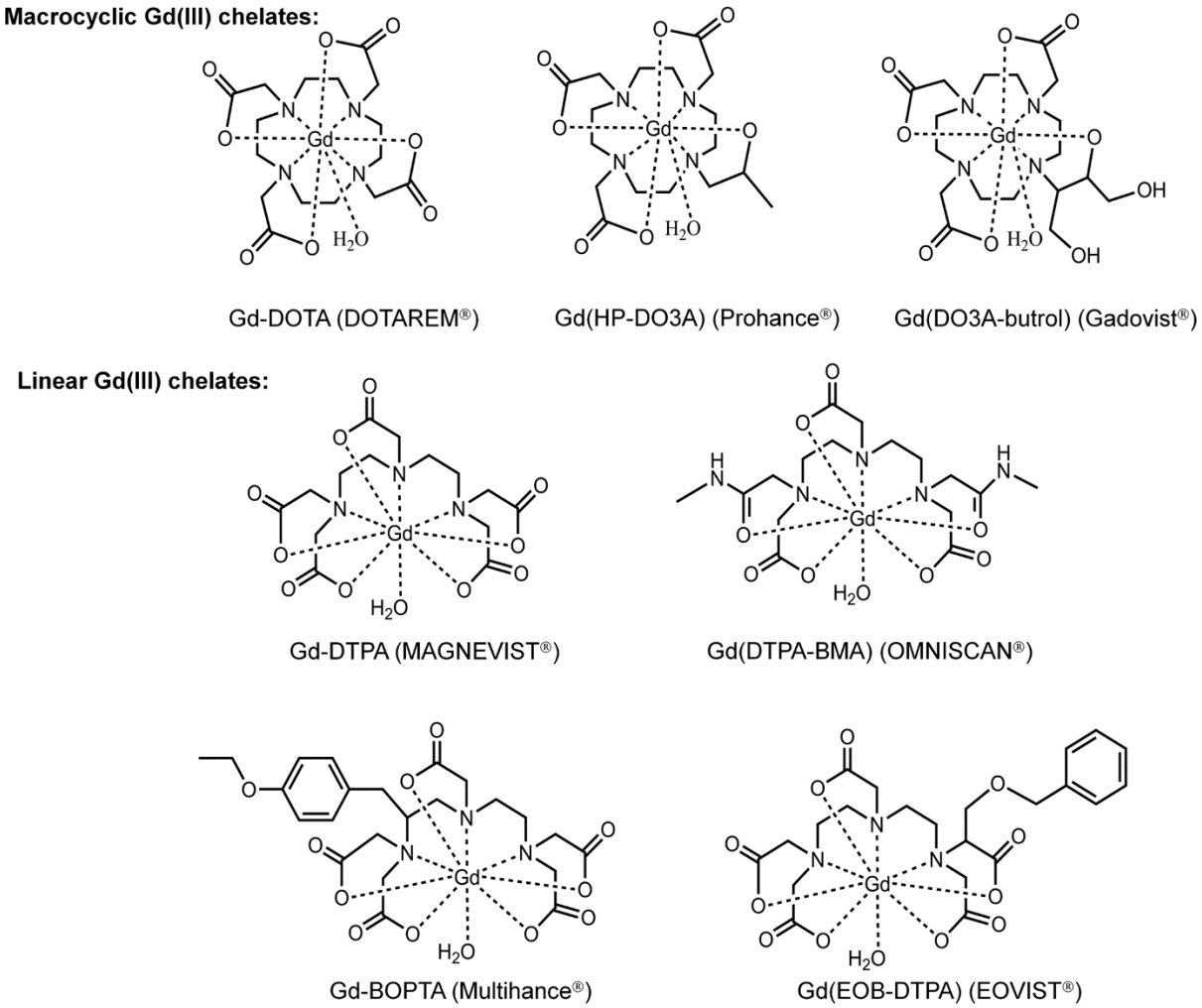

Figure 1.3 Structures of the Gd(III) based MRI contrast agents currently used in the clinical practice.[29]

1.6 Relaxivity and safety of Gd (III)-DOTA

The high relaxation of a contrast agent is vital for effective contrast enhanced MRI. Relaxivity of the contrast agent describes its ability to alter the rate of water proton relaxation. Gd (III)-DOTA contrast agents can increase both T_1 and T_2 relaxation rates ($1/T_{1,2}$) of water protons. The observed water proton relaxation rates include the contributions from the relaxation rates $(1/T_{1,2})_d$ without a contrast agent and the increased relaxation rates $(1/T_{1,2})_p$ by the contrast agent. The increased relaxation rates of water protons are linearly related to the concentration of the contrast agent within the range of clinically relevant concentrations. The realxivity is

defined as the concentration-dependent increase in relaxation rate of water protons by the contrast agent in the units of $mM^{-1}S^{-1}$.

$$\left({}^{1}/_{T_{1,2}}\right)_{obs} = \left({}^{1}/_{T_{1,2}}\right)_{d} + r_{1,2}[\mathrm{Gd}] \qquad (1.1)$$

The relaxivities of traditional small molecular contrast agents can vary if they bind to macromolecules such as plasma proteins or some polysaccharide, for example, fucoidan which is used in our study. For the contrast agents binding to proteins, the relaxivities can change by the concentrations of the agents and plasma proteins [33]. Moreover, the relaxivities are dependent on magnetic field strength [34, 35].

Safety is also a very important element of MRI contrast agent for clinical applications. Gd(III) ions cannot be administered directly because of their high toxicity in ionic form, acutely interfering with calcium channels and protein binding sites.[36, 37] Free Gd ions accumulate in liver, spleen, kidney and bones and have an LD_{50} = 0.2 mmol/kg in mice.[29] Gd(III) ions are complexed with chelating ligands to prevent tissue interaction and minimize toxic side effects. The FDA has issued a black box warning to prohibit the use Gd(III) based contrast agents in the patients with renal malfunctions. Therefore, Gd(III) chelate based MRI contrast agents with good safety profiles should have high thermodynamic and kinetic stability. The contrast agents should be excreted after the contrast enhanced MRI within hours of administration.

1.7 Fucoidan

In this work, P-selectin was chosen as the molecular target. Fucoidan (the typical structures are

shown in **Figure 1.4**) is a sulfated polysaccharide (MW: average 20,000) found mainly in brown algae and brown seaweed. Fucoidan is used as an ingredient in some dietary supplement products.

It has been previously demonstrated in vivo by us and other groups, that fucoidan-functionalized nanoparticles or microparticles targeting P-selectin can be used for the diagnosis of endothelial activation and intraluminal thrombosis, and for tumor-selective drug delivery [5, 38, 39]. Fucoidan refers to a type of highly sulfated polysaccharide containing L-fucose groups [40]. This natural compound exhibits a high affinity for P-selectin, mimicking its main ligand the P-selectin Glycoprotein Ligand 1 (PSGL-1) [41]. Fucoidan has a nanomolar affinity for the P-selectin expressed by activated platelets in the thrombus [8]. We work herein with fucoidan, the P-selectin targeting polysaccharide, linking with dextran, using in vivo click reaction, to achieve specific detection of PDAC tumor xenografts in mice [42].

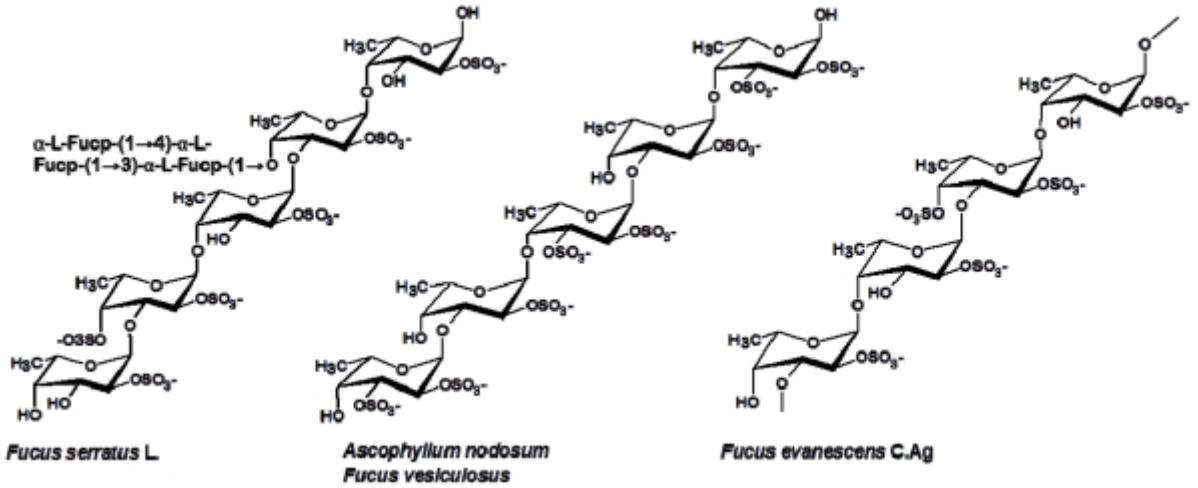

Figure 1.4 Typical structure of fucoidan (FCSPs) obtained from some brown seaweed species in the order of Fucales [43].

1.8 Summary

The aim of this study was to develop multimodality P-selectin-targeted imaging probes using fluorescent dye, gadolinium chelates, superparamagnetic iron oxide particles, and natural dextrans. In the following sections, we describe the synthesis and characterization of these imaging agents. Gadolinium chelates and superparamagnetic iron oxide particles are used for T1- and T2*-weighted MRI and dextrans can be directly detected through its abundant hydroxyl protons by CEST MRI [9, 44]. Development of P-selectin targeted dextrans for CEST MRI, although not tested in the time frame of the thesis project, is the ultimate goal of our study.

2. Experimental Methods

2.1 Synthesis

2.1.1 Materials

Amino-dextran (MW= 500KD), and N, N′-Disuccinimidyl carbonate (MW:256.17, abbr. DSC) and Fucoidan (MW: ~150 KD) were purchased from Sigma Aldrich (Saint Louis, MO, USA). DBCO-NH_2 (MW: 276.3) is acquired from BroadPharm (San Diego, California). NHS-PEG-Azide ($C_{15}H_{24}N_4O_8$ MW: 388.37) is acquired from Thermo Fisher Scientific.

2.1.2 Synthesis Method of Dextran-N_3

Amino-dextran of 0.3 umol (150 mg) is dissolved in 500 uL PBS pH:7.4~8.0, followed by adding 21 umol (8.3mg) NHS-PEG-N_3 （dissolved in 500 uL PBS pH:7.4~8.0）.The mixture is vortexed and allowed to conjugate for 2 hours at room temperature. Excess reactants are removed by dialysis for 1 day. The product is freeze-dried.

2.1.3 Synthesis Method of Fucoidan-DBCO

Fucoidan of 100 mg (0.7 umol) is dissolved in DMSO pH:7.4~8.0. Then, N, N′-Disuccinimidyl carbonate (abbr. DSC) in DMSO (5.1 mg, or 20 umol) and 10 uL triethylamine (abbr. TEA) are slowly added to the solution with pH of 7.4~8.0. The mixture is vortexed and allowed to conjugate for 2 hours at room temperature. The product was then purified by acetone precipitation followed by centrifugation at 4000 rpm in pellets for about 5~10 mins. All of the synthesized Fucoidan-DSC (MW: ~495) is dissolved in 500 uL PBS (pH:7.4~8.0), After that,

we added 27 umol (7.46 mg) DBCO-NH_2 (dissolved in 500 uL DMSO, PH:7.4~8.0) to the solution. The mixture is vortexed and allow to conjugate at room temperature overnight. Excess reactants are removed by dialysis for 1 day. The product is freeze-dried.

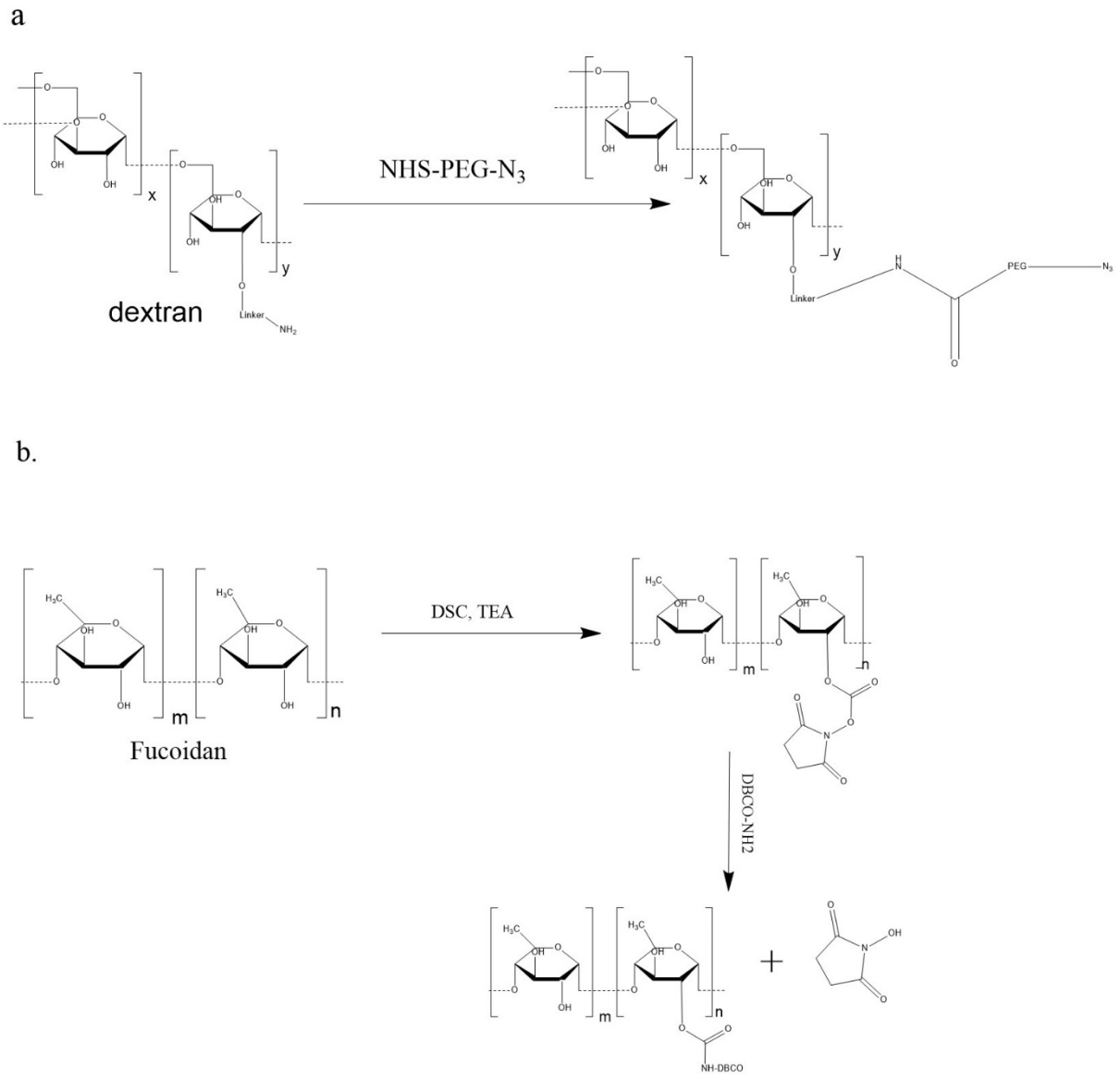

Figure 2.1 Scheme of Synthesis Route of (a) Dextran-N_3 and (b) Fucoidan-DBCO

2.2 In Vitro CEST of Dex10, Dex10-N_3, Fucoidan and Fucoidan-DBCO

2.2.1 Preparation of Samples for MR Imaging

All MRI samples were prepared using 1.5 mL Eppendorf tubes and transferred to 1mm OD capillaries for MRI measurement. The solutions at concentration of 1 mg/mL, were prepared in 10mM phosphate buffered saline (PBS) buffer and titrated to pH=7.4.

2.2.2 MRI Measurement and Analysis

All in vitro MRI datasets were acquired at 37 ℃ (310.15K) on a 400MHz (9.7T) vertical scanner (Bruker Biosciences, Billerica, MA) system equipped with a 20mm birdcage RF coil using a previously reported protocol [45]. A modified single slice Rapid Acquisition with Relaxation Enhancement (RARE) pulse sequence was used to acquire CEST weighted images with saturation offset frequencies from -4 ppm to 4 ppm (step = 0.2 ppm) with respect to water resonance (set 0 ppm by MRI convention). The imaging parameters were, saturation time (T_{sat}) = 3 s, T_R = 10 s, effective T_E = 43.2 ms, RARE factor = 32, slice thickness = 2mm, matrix size = 64x64, resolution = 0.25x0.25 mm^2, and number of averages = 2. The saturation parameters were: rectangular RF pulse, saturation time ($t_{sat)}$ = 1,2,3,4 and 6sec and saturation field strength (B_1) 1.2, 2.4, 3.6, 4.7 and 5.9 μT. The B_0 inhomogeneity was corrected using the WASSAR method.[46, 47]

All data were processed using custom-written Matlab scripts. Conventionally, MTR_{asym} is used to quantify CEST effect by removing other effects from the acquired Z-spectrum, including the

water direct saturation effect and magnetization transfer (MT) effect caused by macromolecules, that are assumed to be symmetric with respect to the water resonance [48]. The definition of MTR_{asym} is given in Equation 2.1.

$$MTR_{asym} = {}^{S_{-\Delta\omega}}/_{S_0} - {}^{S_{+\Delta\omega}}/_{S_0} \tag{2.1}$$

Where Δω is the frequency difference of the protons of interest with respect to the water protons and S and S_0 are the signals acquired with and without saturation, respectively.

To achieve a linear relationship over a broad concentration range, we also adapted the MTR_{rex} metric [49] in our study, which is the reciprocal format of Z-spectral data defined by Equation 2.2.

$$MTR_{rex} = {}^{S_0}/_{S_{\Delta\omega}} - {}^{S_0}/_{S_{-\Delta\omega}} \tag{2.2}$$

To achieve T_1 – relaxation time compensated CEST quantification, we used apparent exchange-dependent relaxation (AREX) metric as defined by Equation 2.3.

$$\text{AREX} = \frac{MTR_{rex}}{T_1} \tag{2.3}$$

Longitudinal (T_1) relaxation times of the samples were assessed using a RARE-based saturation recovery sequence with eight T_R times ranging between 200 ms to 15,000 ms. T_1 relaxation times were estimated by fitting the ROI values to Equation 2.4 using Matlab,

$$\text{S}(T_R) = M_0 - \left[1 - \exp\left(-\frac{T_R}{T_1}\right)\right] \tag{2.4}$$

Where $S(T_R)$ are the MRI signal at each T_R time, and the theoretical maximal MRI signal S_0

and T_1 time are the parameters to be estimated.

In addition, transverse (T_2) relaxation times were measured using the same RARE sequence with a CPMG preparation period inserted before the imaging readout.[50] The inter-echo time delay (τ_{CMPG}) was fixed at 10 ms and the pulse numbers were varied from 4 to 1024. The acquisition time for each T_2-weihted image was 25 sec. T_2 relaxation times were estimated by fitting the ROI values to Equation 2.5 using Matlab,

$$S(T_E) = M_0 \times \exp\left(-\frac{T_E}{T_2}\right) \quad (2.5)$$

Where $S(T_E)$ are the MRI signal at each T_E time, and the theoretical maximal MRI signal M_0 and T_2 time are the parameters to be estimated.

2.3 Histological Analysis of P-selectin Expression in tumor and muscle

2.3.1. Immunohistochemistry (IHC) Staining Protocol

Materials: P-selectin Antibody (CTB201): sc-8419 was purchased from Santa Cruz Biotechnology. P-Selectin Antibody (CTB201) is a mouse monoclonal IgG_1 (**kappa light chain**) provided at 200 µg/ml**.**

The slices are taken from refrigerator (-20 ℃), and they should be kept under room temperature and in dark place. The slices are washed with PBS to remove the optimum cutting temperature medium (OCT) and to allow staining of the tissues. Tissues were permeabilized the tissues with acetone, leave to fix the tissue under -20 ℃ for 10 min. Wetting the slices with PBS, circle the

tissues with hydrophobic marker. Incubating the tissues for 1h in block (BSA), room temperature. It is recommended that as incubations can be very long in whole mount staining, the P-selectin antibody should be diluted in blocking buffer (1:200 in BSA). Washing the slices with PBS 3X5 min in PBS. Add secondary antibody (Anti-Mouse IgG Alexa Fluor 594) in blocking buffer (1:500 in BSA), incubate for 30 min, room temperature. Washing 3X5 min in PBS again. Staining the slices with 1:100 DAPI, incubate for 5 min. Wash in PBS. Mount and view the slices. Store at 4℃ in the dark until analysis

Immunohistochemical localization of P-selectin was determined in tumor and muscles samples after intravital microscopy was completed. For P-selectin channel, we set the minimum intensity was 2640 and the maximum intensity was 56062 to keep the consistent intensity both in tumor and in muscle. We assumed that if the intensity we tested in tumor is higher, then we can prove that P-selectin over expresses in tumor.

2.4 Ex Vivo Fluorescence Imaging

2.4.1 Cell Culture

The murine PDAC KPC cells[42] were derived from $Kras^{LSL.G12D/+}$; $p53^{R172H/+}$; $Pdx^{Cretg/+}$ (or KPC) mice. KPC cells were cultured at 37 °C and 5% CO_2 in RPMI medium supplemented with 10%FBS (100ml), 1% PenStrep (10ml), 1% MEMNEAA (10ml), 1% Sodium Pyruvate (10ml) and 1% L-glutamine (10%).

2.4.2 The KPC Model of Pancreatic Ductal Adenocarcinoma

We utilized a variety of genetically engineered mouse models of pancreatic cancer. However, the principle model utilized in the Mouse Hospital is the $Kras^{LSL.G12D/+}$; $p53^{R172H/+}$; $Pdx^{Cretg/+}$ (or KPC) model, a well-validated, clinically relevant model of PDAC.[51] KPC mice develop a spectrum of premalignant lesions called Pancreatic Intraepithelial Neoplasia (PanINs) that ultimately progresses to overt carcinoma with 100% penetrance. The tumors generally have a moderately differentiated ductal morphology with extensive stromal desmoplasia, similar to the most common morphology observed in humans. Metastases are observed in 80% of KPC mice, primarily in the liver and lungs, the same sites most commonly observed in humans. The tumors exhibit numerous immunohistochemical markers of PDA and harbor complex genomic rearrangements indicative of genomic instability. Furthermore, KPC mice develop the co-morbidities associated with human PDA such as cachexia, jaundice and ascites. Finally, pancreatic tumors in KPC mice are predominantly resistant to chemotherapy, with only 12% of tumors demonstrating a change in growth kinetics after treatment with gemcitabine.[52]

2.4.3 Animal Model

All animal experiments were conducted in compliance to protocols approved by institutional Animal Care and Use Committee of Johns Hopkins University. One million KPC cells (in 200 μL PBS) were subcutaneously injected to both lower flanks of C57BL/6J mice (6–8-week-old females, Jackson Laboratories, USA) to form two tumors (for successful tumorigenesis). Mice were randomly selected for different groups. The investigators were not blinded to the grouping of mice.[42]

2.4.4 Fluorescence Imaging Analysis

We Performed preliminary in vivo testing in subQ tumor model. Examined localization of Cy5.5-azide localization to mice injected with fuoidan-DBCO by ex vivo fluorescence imaging

Materials: 6 mice, Disulfo-Cy5.5 azide (fluorescence, the concentration is 3.815mg/L), Fucoidan-DBCO (in PBS, the concentration is 1mg/200uL)

Experimental Groups: As shown in **Figure2.2**, 40 nmol/kg of Cy5.5-N_3 is in vivo injected at 1 h after injecting fucoidan-DBCO (40 mg/kg), and 1 hour later, dissecting the mice and getting all organs including tumors and muscles, and last examining localization of cy5.5-azide localization to mice by ex-vivo fluorescence imaging.

Control Groups: As shown in **Figure 2.2,** 40 nmol/kg of Cy5.5-N_3 is in vivo injected in mice without fucoidan-DBCO injection. 1 hour later, dissecting and getting all organs including tumors and muscles, and last examined localization of cy5.5-azide localization to mice by ex-vivo fluorescence imaging.

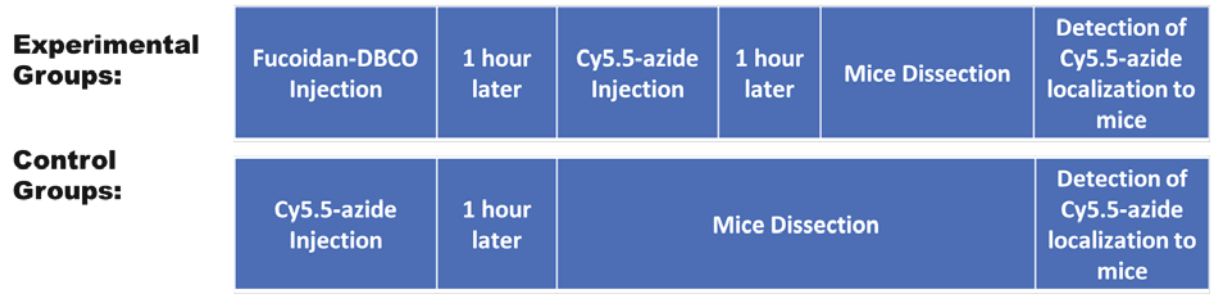

Figure 2.2 Scheme of Ex vivo Fluorescence Imaging.

2.5 Relaxivity of Gd(DOTA)-N_3

High relaxivity of a contrast agent is critical for effective contrast enhanced MRI. Relaxivity of the contrast agent describe its ability in changing water proton relaxation rates. Gd (III)-DOTA-N_3 contrast agents can increase both T_1 and T_2 relaxation rates ($1/T_{1,2}$) of water protons.[53] Hydrophilic Gd (III) contrast agents are primarily used clinically for angiography as they are restricted to the vascular space and therefore can identify damaged blood vessels.[53-55] This concept can be applied to tumor imaging, as most tumors are more perfuse than surrounding tissue.

2.5.1 Chelation Reaction of T_1 Agent Gd(DOTA)-N_3

Materials: Azide-mono-amide-DOTA ($C_{19}H_{34}N_8O_7 \cdot 3HCl$, MW: 595.9, 100mg) was purchased from Macrocyclics, Inc. Gadolinium (III) acetate hydrate ($Gd(CH_3CO_2)_3 \cdot xH_2O$, MW: 334.38, 25g) was purchased from Sigma-Aldrich.

Synthesis Methods: 0.06mol Azide-mono-amide-DOTA and 0.6mol Gadolinium (III) acetate hydrate were dissolved in 10mL DI water, adjust PH = 6.5 with 1M NaOH, oil bath (50 ℃) for 2 days. Purify the product with HPLC. Freeze-drying the purified product.

HPLC Methods: Analytical reverse-phase HPLC-MS was performed on a Varian Prostar 500 system (Agilent Technologies, Santa Clara, CA, USA) with a waters (Milford, MA, USA) Atlantis C_{18} column (4.6×250, 5 μm). This system is equipped with a Varian 380 LC ELSD system, a Varian 363 fluorescence detector, and a Varain 335 UV-vis detector, and a Varian 1200L quadrupole MS detector (Agilent Technologies, Santa Clara. CA, USA). Preparative

runs were performed on a Waters (Milford, MA, USA) Atlantis C_{18} column ($19\times 250, 10\mu m$). The mobile phases consisted of Milipore water (A) and HPLC-grade acetonitrile (B). HPLC method 1:0-5 min 100% A, 5-24:08 min 57.5% A, 24:08-30 min 0% A, 30-35 min 0% A, 35-40 min 100% A.

2.5.2 Chelation of T_2 Agent SPIO-N_3

Materials: SPIO-COOH was purchased from Ocean NanoTech. EDC and NH_2-PEG-N_3 (mw = 3000) was purchased from Sigma-Aldrich.

Synthesis Methods: Equilibrated EDC to room temperature. Prepared 25 mL SPIO-COOH. Dissolved 10 mg EDC and 10 mg NHS in 1 mL PBS respectively. Added 10 μL EDC solution and 10 μL NHS solution, and mixed with SPIO-COOH in PBS, PH 6.5 and reacted for 30 min. Dissolved 25 mg NH_2-PEG-N_3 in 1 mL PBS, added this solution to the former one and reacted for 2 hours, PH 7.4 and room temperature. The product was purified by dialysis.

2.5.3 T_1 and T_2 of Gd(DOTA)-N_3

The efficiency of a contrast agent in reducing the longitudinal relaxation time of water protons is defined in terms of its relaxivity ($mM^{-1}\ s^{-1}$).[56] It has been predicted by Solomon-Bloembergen-Morgan theory that slow molecule tumbling of an MR contrast agent will cause an increase in rotational correlation time, τr, which in turn results in increased relaxivity.[57] One of the common approaches to increasing relaxivity by slowing down the molecular tumbling is to attach Gd(III) complexes to a macromolecule through rigid linkages.[58-61]

The longitudinal relaxivity (r_1) measurements and transverse relaxivity (r_2) measurements are shown as follows.

Prepare a series of samples of Gd(DOTA)-N_3 at different concentrations, such as 0.39 mM, 0.19 mM, 0.097 mM, 0.049 mM, 0.024 mM, and measure the T_1 and T_2 values, respectively. Then, plot of C vs $1/T_1$, and the slop of which will be r_1, plot of C vs $1/T_2$, and the slope of which slope will be r_2.

2.6 In Vivo MRI with Azide-Gd(DOTA)

For in vivo study, the method is shown in **Scheme 2**. We used an 11.7T Bruker Biospec horizontal scanner. T1 and T2 were performed before and after the i.v. injection of 200 uL of fucoidan-DBCO and Azide-Gd(DOTA) solutions in saline (500mg/kg b.w.), using the following parameters: B1 = 1.8 μT, t_{sat} = 3 s, Δω range of -3 to +3 ppm with a step size of 0.2 ppm, T_R/T_E = 5 s/18.6 ms, number of averages = 2, slice number = 1, slice thickness = 1 mm, matrix size = 64 × 64, field of view = 25 mm × 25 mm, total scan time = 5 min for 1 image. The B_0 inhomogeneity maps was acquired before and after the CEST acquisitions using MASSR method using the following parameters: B_1 = 0.5 μT, t_{sat} = 500 ms, Δω range of -1 to +1 ppm with a step size of 0.1 ppm. Equation 2.1 was computed after the B_0 correction. ΔMTR_{asym} at each time point was calculated by MTR_{asym}(t) - MTR_{asym}(pre). Data were processed using custom-written MATLAB programs. T_1 maps were acquired using the same geometry and spatial resolution as CEST MRI with a RARE-VTR sequence (RARE with variable T_Rs, effective T_E = 25 ms and RARE factor = 4) with 12 T_R times ranging from 60 ms to 10 s. Total time of T_1 mapping is 5min for 1 image. T_2 maps were measured using the same geometry and spatial resolution as CEST MRI with a modified Multi Slice

Multi Echo (MSME) method described previously with T_R = 2200 ms and 30 echo times ranging from 7.5 to 225 ms. Total time of T_2 mapping is 4 min 16 s.

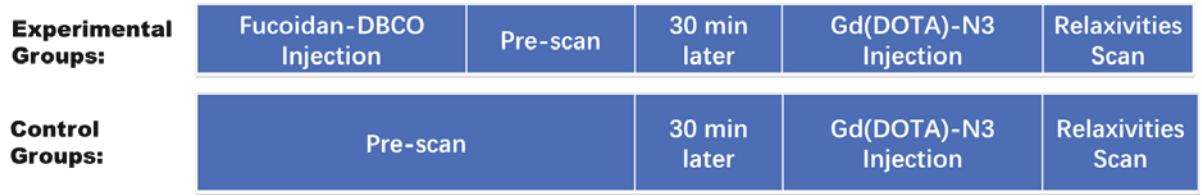

Figure 2.3 Scheme of In Vivo T1 & T2 Scan

3. Results

3.1 Synthesis of Dextran-N_3 and Fucoidan-DBCO

We first conjugated Amino-dextran and NHS-PEG-N_3 to construct CEST agent dextran-N_3 according to the route shown in **Scheme 1(a)**. We got Dextran-N_3 79.5 mg, and after calculation, we got the yield is 53.0%.

We also successfully synthesized fucoidan-DBCO according to the route shown in **Scheme 1(b)**. First, we conjugated fucoidan and N, N′-Disuccinimidyl carbonate (abbr. DSC). Briefly, N, N′-Disuccinimidyl carbonate (DSC) was used to active the hydroxyl groups of fucoidan to form succinimidyl groups. The conjugation of the activated fucoidan was synthesized with DBCO-NH_2 to form fucoidan-DBCO. We got Fucoidan-DBCO 158.4 mg, and after calculation, we got the yield is 58.5%.

Finally, we characterized dextran, dextran-N_3, fucoidan and fucoidan-DBCO using in vitro CEST MRI to prove we successfully synthesized dextran-N_3 and fucoidan-DBCO. The CEST results are shown below.

3.2 In Vitro CEST Results

Figure 3.1 is the in vitro MRI result of fucoidan and dextran. We tested the T2 weighted imaging and CEST imaging, Using the asymmetric magnetization transfer ratio Equation 2.1 to get the MTR_{asym} values and get the plot.

It proved that due to the abundant hydroxyl groups of dextran, the CEST signal is much

stronger than fucoidan, so we use dextran as CEST MRI agent to increase the sensitivity of detection.

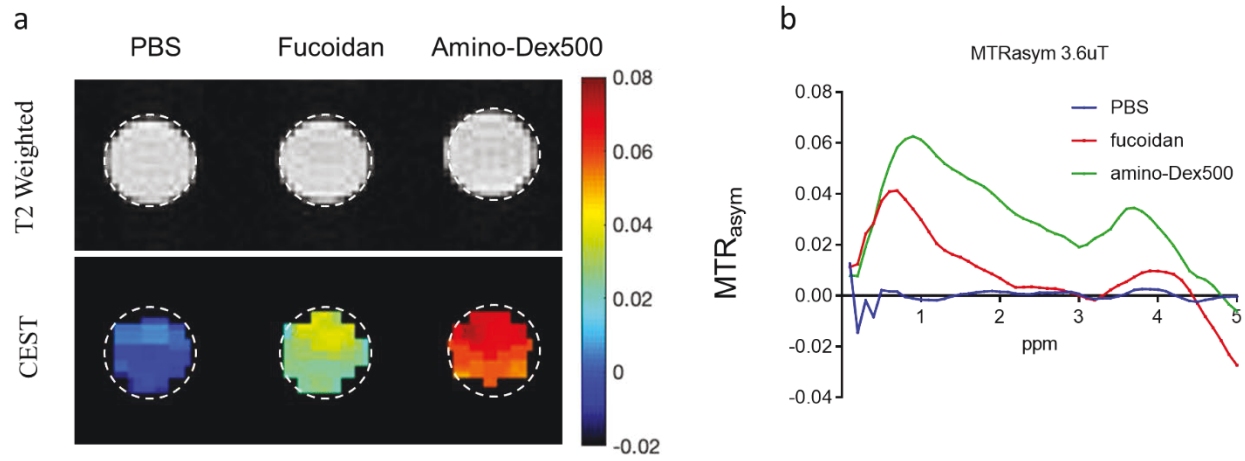

Figure 3.1 In vitro CEST of fucoidan and dextran.

3.3 Histological Analysis of P-selectin Expression in tumor and muscle

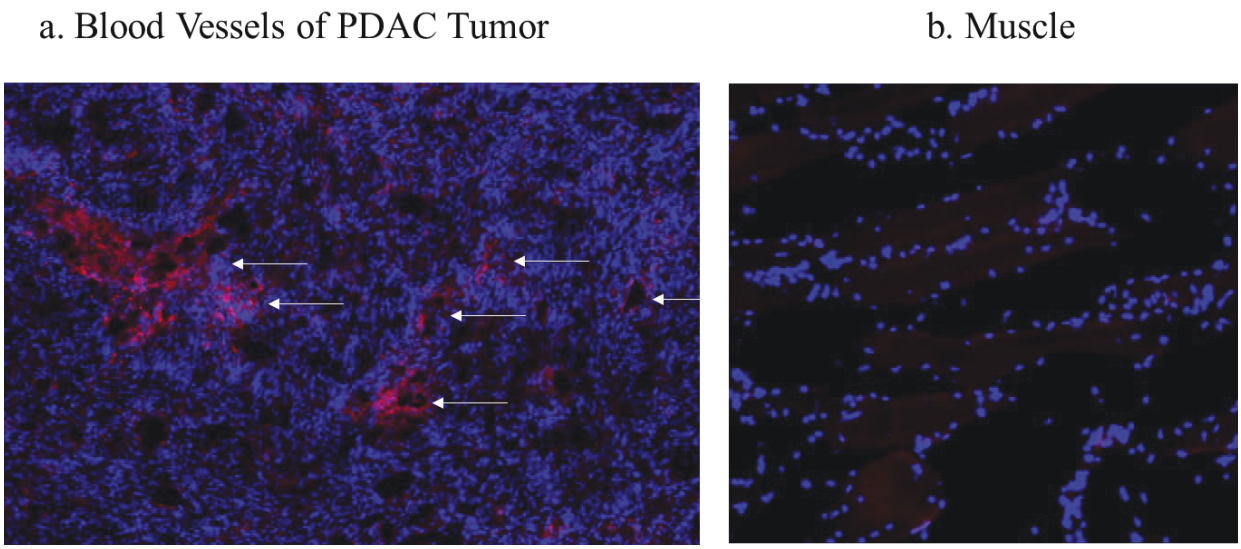

Figure 3.2 Immunohistochemistry (IHC) Analysis of P-selectin Expression in (a) Tumors and (b) Muscles.

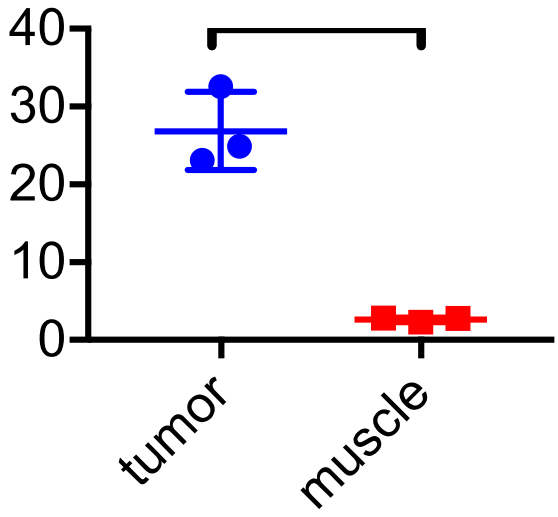

Figure 3.3 Quantification of P-selectin Expression in Tumors and Muscles (N=3, two-tailed unpaired Student's test, based on whole-tumor ROI)

We randomly choose three mice for different groups, and this is the result we got.

Our preliminary inference is P-selectin expresses more in tumor than which in muscle. According to the above **Figure 3.2a** and **Figure 3.2b**, we can see the intensity of P-selectin in tumor is obviously higher than which in muscle. That means P-selectin expression in tumor is much more than which in muscle.

As is shown in **Figure 3.3**, we also made quantitative analysis of fluorescence intensity. The average fluorescence intensity of P-selectin in tumor and in muscle is about 28 and 2 respectively, and the P value is 0.0011(<<0.5), therefore, the result is significant, which means P-selectin expression in tumor is much more than which in muscle. This result fully explain that P-selectin is over expressed in tumor.

3.4 Ex Vivo Fluorescence Imaging

we performed preliminary in vivo testing in subQ tumor model to examine Cy5.5-azide localization to mice injected with fucoidan-DBCO to see the feasibility of later MR Imaging and make dual proof of P-selectin's over expression in tumor.

Sulfo-Cyanine5.5 (**Figure 3.4**) is a water-soluble, hydrophilic fluorophore. As other cyanine dyes, ulfo-Cyanine5.5 has an outstanding molar extinction coefficient which gives rise to its bright fluorescence. The molecule contains four sulfo groups that provide hydrophilicity and negative charge to the fluorophore – this minimizes non-specific binding.

The subcutaneous tumors were formed by implanting syngeneic $Kras^{LSL.G12D/+}$; $p53^{R172H/+}$; $Pdx^{Cretg/+}$ (KPC)-derived PDAC cells[62]. The implantable model shares similar ECM and immunobiology as the parental tumors arising spontaneously in KPC mice, providing a simple and well-controlled model that recapitulates cellular and molecular pathology of human PDAC[63, 64]. To ensure successful tumor formation, two tumors were implanted on both sides of the flank of each mouse subcutaneously (**Figure 3.5**).

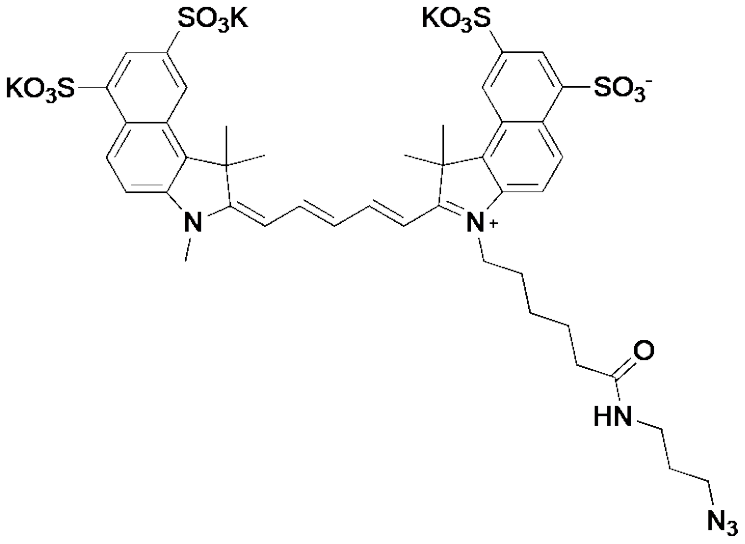

Figure 3.4 Chemical Structure of Sulfo-Cy5.5-N_3

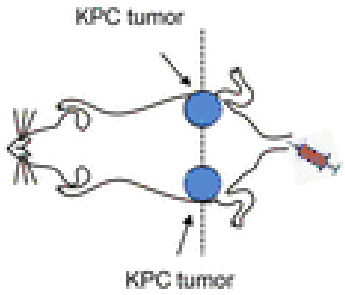

Figure 3.5 Schematic of the tumor position

Our results are shown in **Figure 3.6** and **Figure 3.7.** According to the of fluorescence examination results of control group and experimental group (**Figure 3.6**), we can see the difference between tumor and muscle in experimental groups is bigger than which in the control groups. That proves the high expression of the P-selectin allows a stronger imaging probe accumulation. Biodistribution studies of the fucoidan-based nanoparticles in mice bearing P-selectin expressing tumors found selective tumor accumulation within 24 hours after injection. Apart from the tumors, the organs exhibiting nanoparticle accumulation were the lungs and the liver, with virtually no uptake in the spleen. Although nanoparticles often accumulate in the liver and spleen, often before hepatobiliary clearance, it was previously found that the use of endothelial targets can modulate nanoparticle biodistribution to the lungs, likely due to the large endothelial component in this organ[65].

Besides, after analyzing ROI values of control groups and treatment groups, we got the P value is 0.0484 (<0.05), so we can say the result is significant and this means Fucoidan-DBCO and P-selectin have targeted binding in tumors.

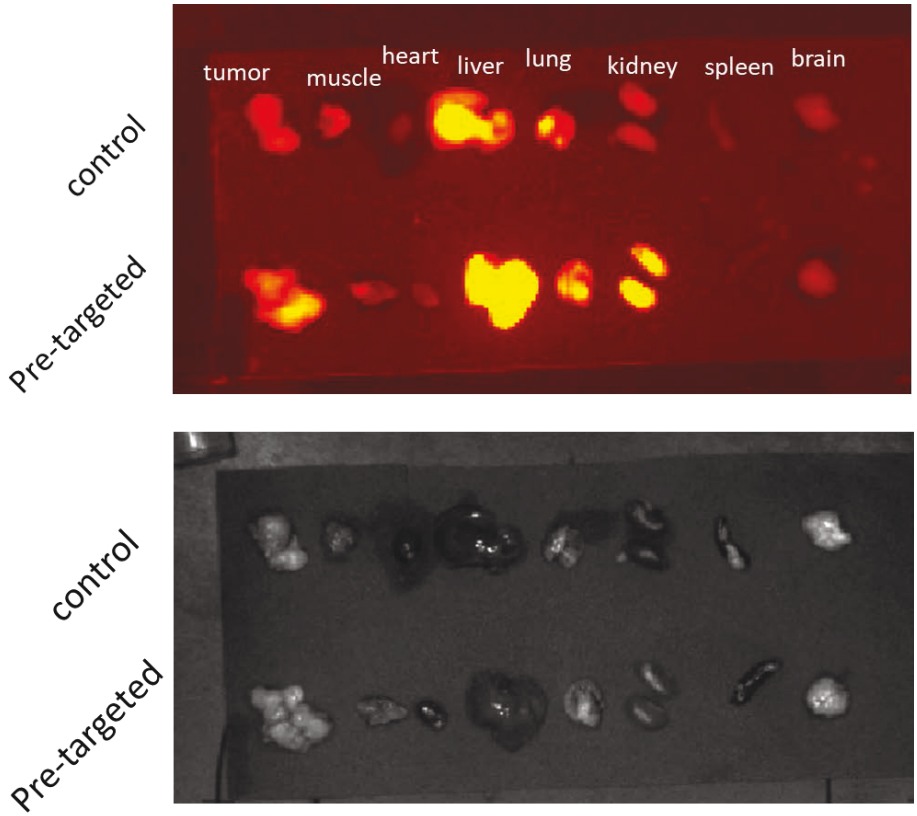

Figure 3.6 Localization of cy5.5-azide localization to mice by ex-vivo fluorescence imaging.

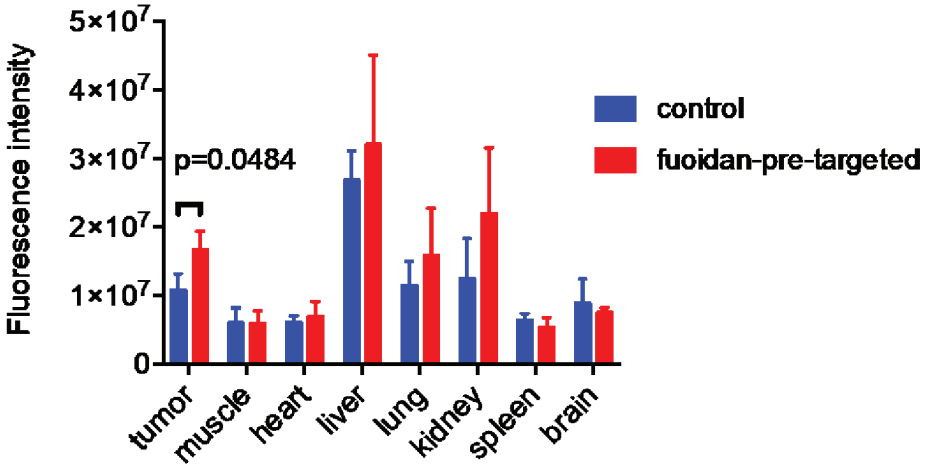

Figure 3.7 Fluorescence Intensity in all organs and muscle and KPC tumor of mice. (N=3, two-tailed unpaired Student's test, based on whole-tumor ROI)

3.5 Relaxivities of Gd(DOTA)-N_3

3.5.1 The productivity of Gd (DOTA)-N_3 Chelation Reaction

We got Gd(DOTA)-N_3 20 mg, the MW of Gd(DOTA)-N_3 is 643.77 g/mol, so the yield is 52.6%.

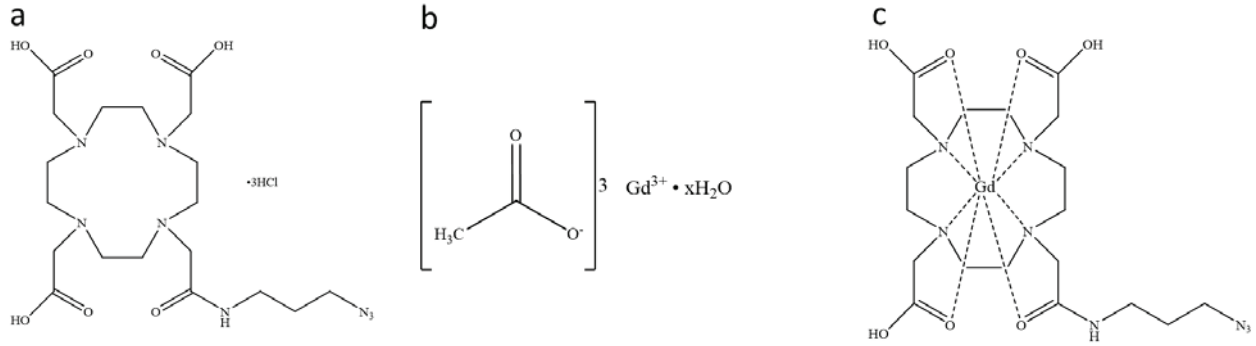

Figure 3.8 (a) Chemical Structure of Azide-mono-amide-DOTA. The chemical name of it is 1,4,7,10-Tetraazacyclododecane-1,4,7-tris (acetic acid)-10-(Azidepropyl ethylacetamide). (b) Chemical structure of Gadolinium (III) acetate hydrate. (c) The chemical structure of Gd (DOTA)-N_3.

3.5.2 The Relaxivities Calculation of Gd (DOTA)-N_3

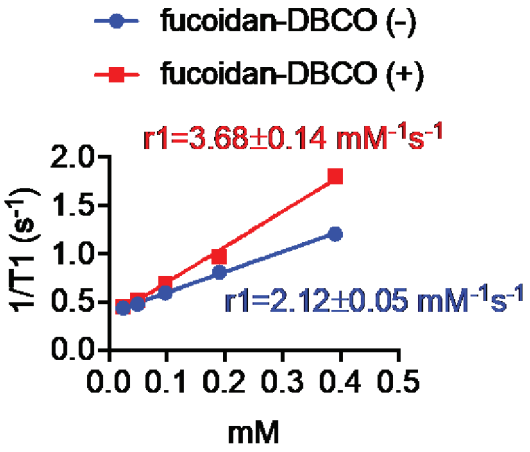

Figure 3.9 R1 relaxation rates of Gd(DOTA)-N_3 with or without adding fucoidan-DBCO.

After calculation, we got r_1=2.12±0.05 $mM^{-1}s^{-1}$ without adding fucoidan-DBCO and 3.68±0.14

$mM^{-1}s^{-1}$ after adding fucoidan-DBCO. The increase of r_1 relaxivty after adding fucoidan-DBCO suggest that the binding of Gd(DOTA)-N3 to fucoidan-DBCO decreased the tumbling rate of the agents, thereby increasing r_1 relaxivty.

3.5.3 In vivo MRI of PDAC using Gd(DOTA)-N_3

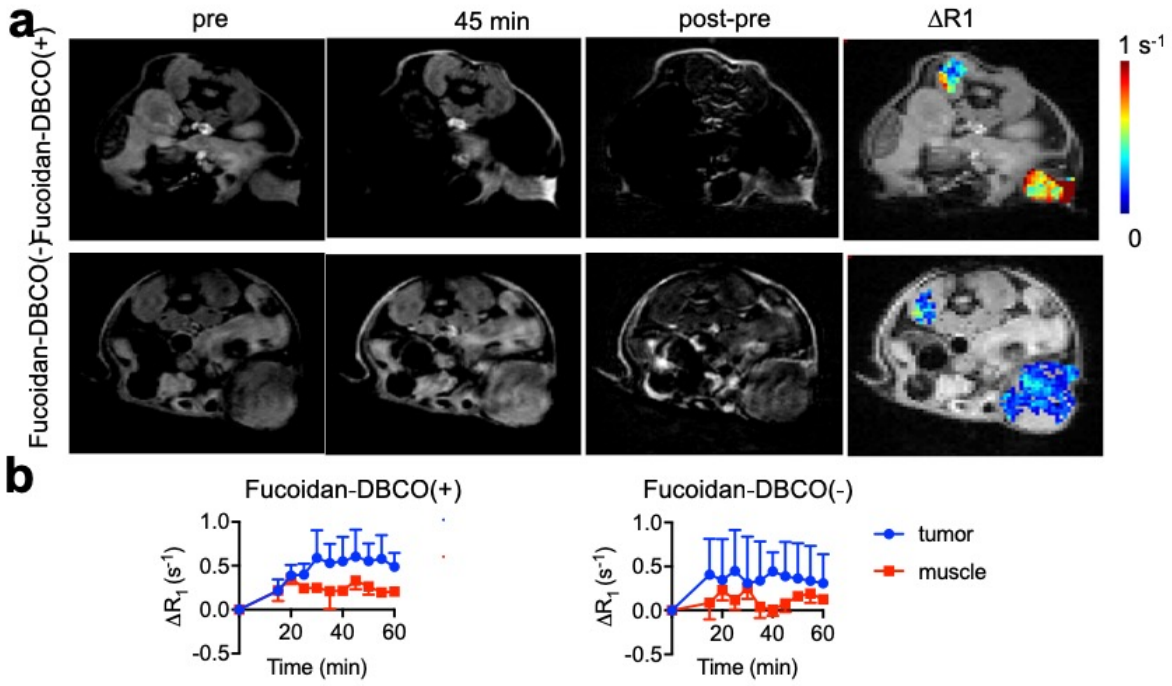

Figure 3.10 (a) T_1-weighted MRI of PDAC using Gd(DOTA)-N_3. (b) Plots of in vivo MRI of tumor and muscle

Gd(DOTA)-N_3 was used for in vivo MRI of PDAC with or without pre-targeting using fucoidan-DBCO at 11.7T. Mice were i.v. injected with 50 mg/kg fucoidan-DBCO. After 1 h, Gd(DOTA)-N_3 was i.v. injected at the dose of 0.2 mmol/kg, during which pre-injection images (pre) and post-injection images up to 1 h were acquired using T1-weighted MRI and T1 mapping. It was shown that mice with fucoidan-DBCO injection demonstrated higher tumor

signal increase in tumor at later times (after 20 min), as revealed by post-pre images and ΔR1 values (N=2). Although we have not acquired sufficient replicates for each group, this data demonstrated the superior tumor enhancement using our platform. More studies would be done to complete the analysis.

4. Discussion

This study aimed for develop versatile platform for multimodality of pancreatic cancer by targeting P-selectin. P-selectin was chosen as a biomarker which is highly overexpressed in the microenvironment of pancreatic tumors[42, 66]. Tumor vasculature, which is composed of smooth muscle cells, pericytes, extracellular matrix, and endothelial cells (ECs), is necessary for the growth and support of tumors. The EC component of tumor neovasculature is a promising target for antitumor therapy because of its genetic stability, exposure to the circulation, and direct access from intravascular space[67]. P-selectin, an inflammatory cell adhesion molecule responsible for leukocyte recruitment and platelet binding[68-71], is expressed constitutively in ECs. It has been found that many human tumors express P-selectin on tumor cells and in tumor vasculature. We found only several reports describing the role of P-selectin as a target for cancer detection and drug delivery[5]. Because of the high prevalence of P-selectin in the microenvironments of human tumors and metastases, as evinced by IHC staining, we surmised that targeting P-selectin may improve early detection of Pancreatic cancer (PDAC).

In this study, we have functionalized fucoidan for in vivo click reaction with imaging moieties to achieve specific detection of PDAC tumor xenografts in mice. We chelated T_1 contrast agent Gd(DOTA)-N_3 and T_2 contrast agents SPIO-N_3, and synthesized CEST agent dextran-N_3. We measured relaxivities of Gd(DOTA)-N_3 in vitro and in vivo and get its contrast enhancement in PDAC tumors. Also, we performed ex vivo fluorescence localization detection to dual prove over expression of P-selectin in tumors and verify the feasibility of later in vivo MR Imaging

to detect PDAC tumor in mice.

In conclusion, in this study, we developed several image probes to bind with fucoidan targeting P-selectin for early detection of pancreatic cancer. Our ultimate goal is to design a new MRI probe for targeted imaging of tumor microenvironment biomarker P-selectin in a murine PDAC model, and this new probe consists of diamagnetic and biocompatible dextran and the high affinity of fucoidan for P-selectin to achieve the specific detection of PDAC tumor.

5. References

1. Segal, R., K. Miller, and A. Jemal, *Cancer statistics, 2018.* CA Cancer J Clin, 2018. **68**: p. 7-30.

2. Heestand, G.M., J.D. Murphy, and A.M. Lowy, *Approach to patients with pancreatic cancer without detectable metastases.* Journal of clinical oncology, 2015. **33**(16): p. 1770-1778.

3. Lee, E.S. and J.M. Lee, *Imaging diagnosis of pancreatic cancer: a state-of-the-art review.* World journal of gastroenterology: WJG, 2014. **20**(24): p. 7864.

4. Saisho, H. and T. Yamaguchi, *Diagnostic imaging for pancreatic cancer: computed tomography, magnetic resonance imaging, and positron emission tomography.* Pancreas, 2004. **28**(3): p. 273-278.

5. Shamay, Y., et al., *P-selectin is a nanotherapeutic delivery target in the tumor microenvironment.* Science translational medicine, 2016. **8**(345): p. 345ra87-345ra87.

6. Mann, A. and T. Tanaka, *E-selectin: its role in cancer and potential as a biomarker.* Transl. Med. S, 2011. **1**: p. 2161-1025.

7. Ryan, U.S. and R.E. Worthington, *Cell-cell contact mechanisms.* Current opinion in immunology, 1992. **4**(1): p. 33-37.

8. Juenet, M., et al., *Thrombolytic therapy based on fucoidan-functionalized polymer nanoparticles targeting P-selectin.* Biomaterials, 2018. **156**: p. 204-216.

9. Ward, K., A. Aletras, and R.S. Balaban, *A new class of contrast agents for MRI based on proton chemical exchange dependent saturation transfer (CEST).* Journal of magnetic resonance, 2000. **143**(1): p. 79-87.

10. Felmlee, J.P. and R.L. Ehman, *Spatial presaturation: a method for suppressing flow artifacts*

and improving depiction of vascular anatomy in MR imaging. Radiology, 1987. **164**(2): p. 559-564.

11. Rosen, B., V. Wedeen, and T. Brady, *Selective saturation NMR imaging.* J Comput Assist Tomogr, 1984. **8**(5): p. 813-818.

12. Van Zijl, P.C. and N.N. Yadav, *Chemical exchange saturation transfer (CEST): what is in a name and what isn't?* Magnetic resonance in medicine, 2011. **65**(4): p. 927-948.

13. Heinze, T., et al., *Functional polymers based on dextran*, in *Polysaccharides Ii*. 2006, Springer. p. 199-291.

14. Soesbe, T.C., Y. Wu, and A. Dean Sherry, *Advantages of paramagnetic chemical exchange saturation transfer (CEST) complexes having slow to intermediate water exchange properties as responsive MRI agents.* NMR in Biomedicine, 2013. **26**(7): p. 829-838.

15. Li, J., et al., *Chemical exchange saturation transfer (CEST) agents: quantum chemistry and MRI.* Chemistry–A European Journal, 2016. **22**(1): p. 264-271.

16. Van Zijl, P.C., et al., *MRI detection of glycogen in vivo by using chemical exchange saturation transfer imaging (glycoCEST).* Proceedings of the National Academy of Sciences, 2007. **104**(11): p. 4359-4364.

17. Walker-Samuel, S., et al., *In vivo imaging of glucose uptake and metabolism in tumors.* Nature medicine, 2013. **19**(8): p. 1067.

18. McMahon, M.T. and A.A. Gilad, *Cellular and Molecular Imaging using Chemical Exchange Saturation Transfer (CEST).* Topics in magnetic resonance imaging: TMRI, 2016. **25**(5): p. 197.

19. Lock, L.L., et al., *One-component supramolecular filament hydrogels as theranostic label-*

free magnetic resonance imaging agents. ACS nano, 2017. **11**(1): p. 797-805.

20. Ngen, E.J., et al., *Imaging the DNA alkylator melphalan by CEST MRI: an advanced approach to theranostics.* Molecular pharmaceutics, 2016. **13**(9): p. 3043-3053.

21. Li, Y., et al., *CEST theranostics: label-free MR imaging of anticancer drugs.* Oncotarget, 2016. **7**(6): p. 6369.

22. Aime, S., et al., *Iopamidol: exploring the potential use of a well-established X-ray contrast agent for MRI.* Magnetic Resonance in Medicine: An Official Journal of the International Society for Magnetic Resonance in Medicine, 2005. **53**(4): p. 830-834.

23. Jones, K.M., et al., *Clinical translation of tumor acidosis measurements with AcidoCEST MRI.* Molecular Imaging and Biology, 2017. **19**(4): p. 617-625.

24. Liu, G., et al., *A dextran-based probe for the targeted magnetic resonance imaging of tumours expressing prostate-specific membrane antigen.* Nature biomedical engineering, 2017. **1**(12): p. 977.

25. Li, Y., et al., *Characterization of tumor vascular permeability using natural dextrans and CEST MRI.* Magnetic resonance in medicine, 2018. **79**(2): p. 1001-1009.

26. Raimondi, S., et al., *Pancreatic cancer in chronic pancreatitis; aetiology, incidence, and early detection.* Best practice & research Clinical gastroenterology, 2010. **24**(3): p. 349-358.

27. Caravan, P., et al., *Gadolinium (III) chelates as MRI contrast agents: structure, dynamics, and applications.* Chemical reviews, 1999. **99**(9): p. 2293-2352.

28. Kuo, P.H., et al., *Gadolinium-based MR contrast agents and nephrogenic systemic fibrosis.* Radiology, 2007. **242**(3): p. 647-649.

29. Zhou, Z. and Z.R. Lu, *Gadolinium-based contrast agents for magnetic resonance cancer*

imaging. Wiley Interdisciplinary Reviews: Nanomedicine and Nanobiotechnology, 2013. **5**(1): p. 1-18.

30. Gallo, J., et al., *CXCR4-targeted and MMP-responsive iron oxide nanoparticles for enhanced magnetic resonance imaging.* Angewandte Chemie International Edition, 2014. **53**(36): p. 9550-9554.

31. Weinmann, H.-J., et al., *Characteristics of gadolinium-DTPA complex: a potential NMR contrast agent.* American journal of roentgenology, 1984. **142**(3): p. 619-624.

32. Torchilin, V., *Tumor delivery of macromolecular drugs based on the EPR effect.* Advanced drug delivery reviews, 2011. **63**(3): p. 131-135.

33. Caravan, P., et al., *The interaction of MS-325 with human serum albumin and its effect on proton relaxation rates.* Journal of the American Chemical Society, 2002. **124**(12): p. 3152-3162.

34. Rohrer, M., et al., *Comparison of magnetic properties of MRI contrast media solutions at different magnetic field strengths.* Investigative radiology, 2005. **40**(11): p. 715-724.

35. Caravan, P., *Strategies for increasing the sensitivity of gadolinium based MRI contrast agents.* Chemical Society Reviews, 2006. **35**(6): p. 512-523.

36. Lansman, J.B., *Blockade of current through single calcium channels by trivalent lanthanide cations. Effect of ionic radius on the rates of ion entry and exit.* The Journal of general physiology, 1990. **95**(4): p. 679-696.

37. Biagi, B.A. and J.J. Enyeart, *Gadolinium blocks low-and high-threshold calcium currents in pituitary cells.* American Journal of Physiology-Cell Physiology, 1990. **259**(3): p. C515-C520.

38. Bonnard, T., et al., *Abdominal aortic aneurysms targeted by functionalized polysaccharide*

microparticles: a new tool for SPECT imaging. Theranostics, 2014. **4**(6): p. 592.

39. Suzuki, M., et al., *Ultrasmall superparamagnetic iron oxide nanoparticles coated with fucoidan for molecular MRI of intraluminal thrombus.* Nanomedicine, 2015. **10**(1): p. 73-87.

40. Chollet, L., et al., *Fucoidans in nanomedicine.* Marine drugs, 2016. **14**(8): p. 145.

41. Bachelet, L., et al., *Affinity of low molecular weight fucoidan for P-selectin triggers its binding to activated human platelets.* Biochimica et Biophysica Acta (BBA)-General Subjects, 2009. **1790**(2): p. 141-146.

42. Han, Z., et al., *An extradomain-B fibronectin-targeted dextran-based CEST MRI probe for detecting pancreatic cancer.* Bioconjugate chemistry, 2019.

43. Ale, M.T., J.D. Mikkelsen, and A.S. Meyer, *Important determinants for fucoidan bioactivity: A critical review of structure-function relations and extraction methods for fucose-containing sulfated polysaccharides from brown seaweeds.* Marine drugs, 2011. **9**(10): p. 2106-2130.

44. Cobb, J.G., et al., *Exchange-mediated contrast in CEST and spin-lock imaging.* Magnetic resonance imaging, 2014. **32**(1): p. 28-40.

45. Ryoo, D., *Label Free CEST MRI Detection of Hydrogen Peroxide and its Applications in Monitoring Oxygen Delivery for Tissue Engineering*. 2017, Johns Hopkins University.

46. Liu, G., et al., *High-throughput screening of chemical exchange saturation transfer MR contrast agents.* Contrast media & molecular imaging, 2010. **5**(3): p. 162-170.

47. Kim, M., et al., *Water saturation shift referencing (WASSR) for chemical exchange saturation transfer (CEST) experiments.* Magnetic Resonance in Medicine: An Official Journal of the International Society for Magnetic Resonance in Medicine, 2009. **61**(6): p. 1441-1450.

48. Liu, G., et al., *Nuts and bolts of chemical exchange saturation transfer MRI.* NMR in

Biomedicine, 2013. **26**(7): p. 810-828.

49. Zaiss, M., et al., *Inverse Z-spectrum analysis for spillover-, MT-, and T1-corrected steady-state pulsed CEST-MRI–application to pH-weighted MRI of acute stroke.* NMR in biomedicine, 2014. **27**(3): p. 240-252.

50. Yadav, N.N., et al., *Natural D-glucose as a biodegradable MRI relaxation agent.* Magnetic resonance in medicine, 2014. **72**(3): p. 823-828.

51. Hingorani, S.R., et al., *Trp53R172H and KrasG12D cooperate to promote chromosomal instability and widely metastatic pancreatic ductal adenocarcinoma in mice.* Cancer cell, 2005. **7**(5): p. 469-483.

52. Olive, K.P., et al., *Inhibition of Hedgehog signaling enhances delivery of chemotherapy in a mouse model of pancreatic cancer.* Science, 2009. **324**(5933): p. 1457-1461.

53. Trivedi, E.R., et al., *Synthesis and characterization of a porphyrazine–Gd (III) MRI contrast agent and in vivo imaging of a breast cancer xenograft model.* Contrast media & molecular imaging, 2014. **9**(4): p. 313-322.

54. Colosimo, C., R. Manfredi, and T. Tartaglione, *Contrast enhancement issues in the MR evaluation of the central nervous system.* European radiology, 1997. **7**(5): p. S231-S237.

55. Roberts, T., N. Chuang, and H. Roberts, *Neuroimaging: do we really need new contrast agents for MRI?* European journal of radiology, 2000. **34**(3): p. 166-178.

56. Merbach, A.S., *The chemistry of contrast agents in medical magnetic resonance imaging*. 2013: John Wiley & Sons.

57. Tóth, É., L. Helm, and A.E. Merbach, *Relaxivity of MRI contrast agents*, in *Contrast Agents I*. 2002, Springer. p. 61-101.

58. Song, Y., et al., *Synthesis and characterization of new porphyrazine-Gd (III) conjugates as multimodal MR contrast agents.* Bioconjugate chemistry, 2010. **21**(12): p. 2267-2275.

59. Prasuhn Jr, D.E., et al., *Viral MRI contrast agents: coordination of Gd by native virions and attachment of Gd complexes by azide–alkyne cycloaddition.* Chemical Communications, 2007(12): p. 1269-1271.

60. Datta, A., et al., *High Relaxivity Gadolinium Hydroxypyridonate− Viral Capsid Conjugates: Nanosized MRI Contrast Agents1.* Journal of the American Chemical Society, 2008. **130**(8): p. 2546-2552.

61. Song, Y., E.K. Kohlmeir, and T.J. Meade, *Synthesis of multimeric MR contrast agents for cellular imaging.* Journal of the American Chemical Society, 2008. **130**(21): p. 6662-6663.

62. Beatty, G.L., et al., *Exclusion of T cells from pancreatic carcinomas in mice is regulated by Ly6Clow F4/80+ extratumoral macrophages.* Gastroenterology, 2015. **149**(1): p. 201-210.

63. Mazur, P.K. and J.T. Siveke, *Genetically engineered mouse models of pancreatic cancer: unravelling tumour biology and progressing translational oncology.* Gut, 2012. **61**(10): p. 1488-1500.

64. Lee, J.W., et al., *Genetically Engineered Mouse Models of Pancreatic Cancer: The KPC Model (LSL-KrasG12D/+; LSL-Trp53R172H/+; Pdx-1-Cre), Its Variants, and Their Application in Immuno-oncology Drug Discovery.* Current protocols in pharmacology, 2016. **73**(1): p. 14.39. 1-14.39. 20.

65. Shuvaev, V.V., J.S. Brenner, and V.R. Muzykantov, *Targeted endothelial nanomedicine for common acute pathological conditions.* Journal of Controlled Release, 2015. **219**: p. 576-595.

66. Lee, H.S. and S.W. Park, *Systemic chemotherapy in advanced pancreatic cancer.* Gut and

liver, 2016. **10**(3): p. 340.

67. Curnis, F., A. Sacchi, and A. Corti, *Improving chemotherapeutic drug penetration in tumors by vascular targeting and barrier alteration.* The Journal of clinical investigation, 2002. **110**(4): p. 475-482.

68. Kansas, G.S., *Selectins and their ligands: current concepts and controversies.* Blood, 1996. **88**(9): p. 3259-3287.

69. Läubli, H. and L. Borsig. *Selectins promote tumor metastasis*. in *Seminars in cancer biology*. 2010. Elsevier.

70. Erpenbeck, L. and M.P. Schön, *Deadly allies: the fatal interplay between platelets and metastasizing cancer cells.* Blood, 2010. **115**(17): p. 3427-3436.

71. Amano, H., et al., *Angiotensin II type 1A receptor signaling facilitates tumor metastasis formation through P-selectin–Mediated interaction of tumor cells with platelets and endothelial cells.* The American journal of pathology, 2013. **182**(2): p. 553-564.

Jiaqi Lu

110w. 39th St, Apt1502 | ljiaqi1@jhu.edu | (443)714-0956

EDUCATION

Johns Hopkins University **08/2017-05/2019**
Master of Engineering in Chemical and Biomolecular Engineering

Zhejiang University **09/2012-07/2016**
Bachelor of Science in Chemistry

PUBLICATIONS & CONFERENCE

1. J. Zhang, Z. Han, **J. Lu**, Y. Li, X. Liao, PCM van Zijl, X Yang, G Liu. Triazoles as T2-exchange MRI contrast agents for the detection of nitrilase activity, *Chem. Eur. J.*, 24, 15013-15018. 2018
2. **J. Lu**, Z. Han, J.Zhang, Y. Li , J. Liu , K. Fujiwara , P. van Zijl , L. Zhang , and G. Liu. Dextran-based CEST MRI for detecting extradomain-B fibronectin in pancreatic cancer. ISMRM 2019 in Montreal, QC, Canada.

RESEARCH EXPERIENCE

Johns Hopkins University

A Versatile Platform for Multimodality Imaging of Pancreatic Tumor by Targeting P-selectin
Advisor: Guanshu Liu, PhD 07/2018-Present

Aims: Develop targeted dextran polymers as MR molecular imaging agents for early detection of pancreatic cancer (PDAC). Dextran polymers are highly biocompatible diamagnetic agent, the abundant hydroxyl protons of which are detectable in chemical exchange saturation transfer (CEST) MRI. Dextran polymers were linked to fucoidan, a P-selectin targeting polysaccharide, using in vivo click reaction, to achieve specific detection of PDAC tumor xenografts in mice.

- Synthesized fucoidan-DBCO and dextran-azide for in vivo click reaction.
- Evaluated the CEST signal of fucoidan-DBCO and dextran-azide in Bruker 400MHz vertical scanner.
- Performed preliminary in vivo testing in subQ tumor model derived from $Kras^{LSL.G12D/+}$; $p53^{R172H/+}$; $Pdx^{Cretg/+}$ (KPC). Examined localization of Cy5.5-azide localization to mice injected with fuoidan-DBCO by ex vivo fluorescence imaging

Triazoles as $T_{2\text{-}Exchange}$ MRI Contrast Agents for the Detection of Nitrilase Activity
Advisor: Guanshu Liu, PhD 09/2017-05/2018

Aims: Develop triazoles as sensitive and tunable diagnostic $T_{2\text{-exchange}}$ agents in MRI.

- Characterized the T2-exchange (T2ex) MRI contrast of azole protons that have large chemical shifts from the water proton resonance as a function of pH, temperature, and chemical modification.
- Studied exchange rates using the Swift-Connick equation to optimize the T2ex effect.
- Applied T2-exchange MRI to assess the activity of nitrilase, an enzyme catalyzing the hydrolysis of 1,2,4-triazole-3-carbonitrile to 1,2,4-triazole-3-carboxylic acid, resulting

in the enhancement of R2ex.

Technical Institute of Physics & Chemistry, Chinese Academy of Sciences

Features and Disbanding of Hydrogen Bands of Cellulose Chains

Advisor: Yong Huang, PhD 09/2016

- Researched on the reconstruction process and control factors of hydrogen bonding between the hydroxyl groups on cellulose macromolecular chains.
- Explored the relationship between the reconstruction of the hydrogen bond and the properties of cellulose macromolecules.
- Investigated the effects of small molecules on cellulose intermolecular and intramolecular hydrogen bond by FTIR, NMR, DSC and QCM.

Structure and Responsibility of Dual-stimuli Sensitive Cellulose Based Graft Copolymers

Advisor: Yong Huang, PhD 01/2015-03/2015

- Synthesized the HPC-g-PDPAEMA graft copolymers with well-defined structure through the atom transfer radical polymerization (ATRP).
- Tested the copolymer's dual sensitivity of pH and temperature in aqueous solution.

Zhejiang University

Diversity Oriented Synthesis Based on Natural Phenolic Compound

Advisor: Jun Wu, PhD *Undergraduate Thesis* 12/2015-06/2016

- Consulted relevant documents and materials and then wrote the literature translation, literature review and research proposals.
- Synthesized salicylaldehyde with 8 different kinds of aromatic amines and aliphatic amines material.
- Recrystallized the products and separated the products with column chromatography
- Characterized the structure of the products by nuclear magnetic resonance and tested the biological activity of the products.
- Analyzed experimental data, wrote a thesis and finally completed thesis defense.

TECHNICAL SKILLS

Experimental Skills: proficient in a variety of chemical experimental instruments and measuring methods such as IR, UV, NMR, FTIR, NMR, DSC, QCM, and MRI
Proficient in Origin, Nova, Chemdraw, TopSpin, GraphPadPrism, Endnote, C Language